Manuscript submitted to
AIMS' Journals
Volume **X**, Number **0X**, XX **200X**

doi:10.3934/xx.xx.xx.xx

pp. **X–XX**

A DYNAMIC THEORY FOR CONTACT ANGLE HYSTERESIS ON CHEMICALLY ROUGH BOUNDARY

Xiao-Ping Wang*

Department of Mathematics, The Hong Kong University of Science and Technology, Clear Water Bay, Kowloon, Hong Kong, China

Xianmin Xu

LSEC, Institute of Computational Mathematics and Scientific/Engineering Computing, NCMIS, Chinese Academy of Sciences, Beijing 100080, China.

(Communicated by the associate editor name)

Abstract. We study the interface dynamics and contact angle hysteresis in a two dimensional, chemically patterned channel described by the Cahn-Hilliard equation with a relaxation boundary condition. A system for the dynamics of the contact angle and contact point is derived in the sharp interface limit. We then analyze the behavior of the solution using the phase plane analysis. We observe the stick-slip of the contact point and the contact angle hysteresis. As the size of the pattern decreases to zero, the stick-slip becomes weaker but the hysteresis becomes stronger in the sense that one observes either the advancing contact angle or the receding contact angle without any switching in between. Numerical examples are presented to verify our analysis.

Dedicated to the memory of Paul Fife

1. **Introduction.** Contact angle hysteresis (CAH) is one of the most important phenomena in the wetting of liquid droplets on surfaces. It plays a crucial role in many applications and industrial processes[1]. Despite its relevance, there is a lack of consensus on how to incorporate a description of contact angle hysteresis into physical models.

The static contact angle is a fundamental concept that characterizes wetting property of the solid surface, which is defined as the measurable angle that a liquid makes with a solid. The contact angle of liquid with a flat, homogenous surface is given by the Young's equation [2]

$$\cos\theta_e = \frac{\gamma_{SV} - \gamma_{SL}}{\gamma}, \tag{1}$$

where γ_{SV}, γ_{SL} and γ denote the interfacial energy of the solid-vapor interface, the solid-liquid interface and the liquid-vapor interface respectively (see Fig. 1). Experimentally, the contact angle of a drop on rough surface has been observed to take a range of values. The highest (lowest) stable contact angle is termed the advancing (receding) angle θ_a (θ_r). The contact angle hysteresis (CAH) $\Delta\theta = \theta_a - \theta_r$ proves to be an important quantity that determines many properties of the

2010 *Mathematics Subject Classification.* Primary: 41A60, 34A36; Secondary: 76T10.

Key words and phrases. Contact angle hysteresis, Cahn-Hilliard equation, asymptotic analysis.

This publication was supported in part by the Hong Kong RGC-GRF grants 605513 and 605311, Hong Kong RGC-CRF grant C6004-14G and NSFC grant 11571354.

* Corresponding author: Xiao-Ping Wang.

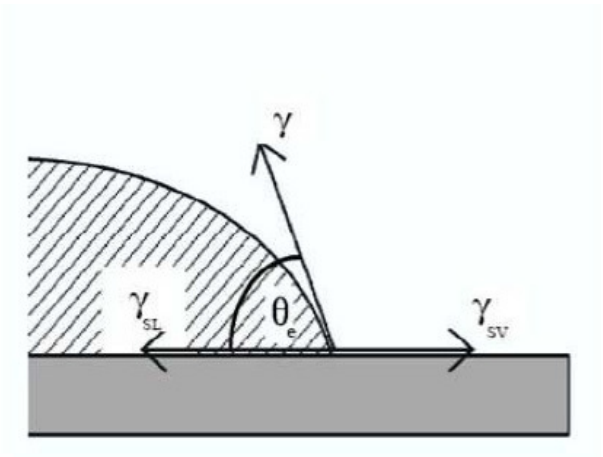

FIGURE 1. Contact angle formed by the liquid-air interface with the solid boundary

surface. The origin of CAH is attributed to several factors such as surface roughness, chemical contaminants, among others. Theoretical models of CAH have focused on roughness and heterogeneity as providing energy barriers for the system to attain the global minimum[3, 4].

In [5], we studied contact angle hysteresis by considering the quasi-static motion of the interface in a channel with chemically patterned boundaries. In this simple geometry, one can follow the change of energy landscape, which also reveals the mechanism for the stick-slip motion of the interface and contact angle hysteresis on the chemically patterned surfaces. As the interface passes through patterned surfaces, we observe not only the stick-slip of the interface and switching of the contact angles, but also the hysteresis of contact point and contact angle.

In this paper, we consider the motion of the interface in a horizontal channel (i.e. $\Omega = (0, L) \times (-H, H)$) with periodically patterned surface modelled by the Cahn-Hilliard equation

$$\varepsilon(\phi_t + U\phi_x) = \Delta\mu, \qquad \mu = -\varepsilon\Delta\phi + \frac{1}{\varepsilon}F'(\phi) \tag{2}$$

with an initial condition $\phi(\mathbf{x}, 0) = \psi(\mathbf{x})$ and boundary conditions on the upper and bottom boundaries $(0, L) \times \{y = -H, H\}$ given by

$$\partial_{\mathbf{n}}\mu = 0, \qquad \varepsilon\phi_t = -\alpha[\varepsilon\partial_{\mathbf{n}}\phi + \gamma'(\phi, x)], \tag{3}$$

and boundary conditions on the left and right boundaries $\{x = 0, L\} \times (-H, H)$ given by

$$\partial_{\mathbf{n}}\mu = 0, \quad \phi = -1 \quad \text{at } x = 0 \tag{4}$$

$$\partial_{\mathbf{n}}\mu = 0, \quad \phi = 1 \quad \text{at } x = L \tag{5}$$

where $' = \partial/\partial\phi$, $\partial_{\mathbf{n}} = \mathbf{n} \cdot \nabla$, and $\mathbf{n}$ is the unit exterior normal to the boundary $\partial\Omega$ of a bounded domain $\Omega \subset R^2$; ε is a small parameter that measures the interface thickness; ϕ is the composition field; $F(\phi) = \frac{(1-\phi^2)^2}{4}$ is the standard double-well function and $\gamma(\phi, x) = \ell(\phi)\cos(\theta_Y(x))$ with $\ell(\phi) = \frac{\sigma}{4}(3\phi - \phi^3)$ and

$\sigma = \int_{-1}^{1} \sqrt{2F(s)}ds = \frac{2\sqrt{2}}{3}$. We assume the static contact angle $\theta_Y(x)$ to be x dependent which allows for a chemically rough surface. We introduce a convection term with a constant velocity U in order to study the dynamics of the interface and contact point. With the boundary conditions (4) (5), we can assume there is an interface separating one phase ($\phi = -1$) on the left of the channel from another phase ($\phi = 1$) on the right. We consider the problem (2) in a time interval $[0, T^*)$ such that $0 < T^*U < c_0$ for some c_0 so that the interface remains inside the channel.

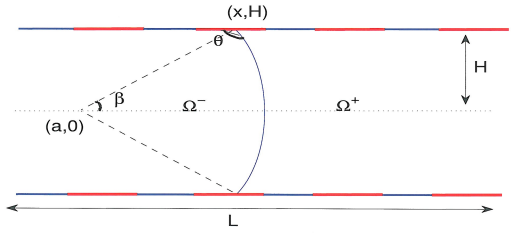

FIGURE 2. Interface motion in a channel

The relaxation boundary condition is part of the boundary conditions proposed in[6, 7, 8] for the phase field model for the moving contact line. In the case of slow interface motion, we can neglect the Navier-Stokes equation and the phase field model is reduced to the Cahn-Hilliard equation with the relaxation boundary condition. The well-posedness of (2) with the relaxation boundary condition is studied in [9]. The dynamics of the contact point and the contact angle are also derived in the sharp interface limit.

To study the interface dynamics and contact angle hysteresis, we use the method of matched asymptotic expansions to derive a system of equations for the dynamics of contact point $x(t)$ (the x coordinate) and contact angle $\theta(t)$ in the sharp interface limit ($\epsilon \to 0$):

$$\begin{cases} \theta_t = \left[\alpha \frac{\cos\theta - \cos(\theta_Y(x))}{\sin\theta} + v\right] \tilde{g}(\theta), \\ x_t = -\alpha \frac{\cos\theta - \cos(\theta_Y(x))}{\sin\theta}, \end{cases} \tag{6}$$

where $\tilde{g}(\theta) = \frac{\cos^3(\theta)}{\cos\theta + (\theta - \frac{\pi}{2})\sin\theta}$, $\theta_Y(x)$ is the local Young's angle and v is the velocity of the moving interface. Phase plane analysis of the system (6) reveals the mechanism for the stick-slip motion of the interface and contact angle hysteresis on the chemically patterned surface (i.e. $\theta_Y(x)$ is a periodic piecewise contant function). When the speed of the interface motion approaches zero, the results are consistent with the quasi-static analysis in [5]. Direct numerical simulations are also performed and the results compared well with the analytical results.

The outline of the paper is as follows. In Section 2, we derive the dynamic equations for contact angle and contact point using multiscale expansions. In Section 3, we study the behavior of the solutions of the ODE system by phase-plane analysis. Finally, in Section 4, we give some numerical examples to verify our analysis results.

2. **Derivation of the dynamic contact angle equation.** We first derive the energy estimate for the model equation. Integrate the equation (2) and use the

boundary conditions, we can easily obtain,

$$\frac{d}{dt}\int_\Omega \phi\, d\mathbf{x} + (4H)U = 0 \tag{7}$$

To study the behavior of the solution as $\varepsilon \to 0$, we then derive the energy estimate for the above Cahn-Hilliard equation. We make a mild assumption that, for $0 < t < T^*$,

$$\left|\int_{\{x=0\}} \mu dy + \int_{\{x=L\}} \mu dy\right| < c_1,$$

for some constant c_1. In [9], we show that solution ϕ is uniformly bounded for our choice of $F(\phi)$. This gives the estimate $\int_\Omega \mu\phi_x d\mathbf{x} \le c_1 + c_2\int_\Omega |\nabla\mu|^2 d\mathbf{x}$. We then multiply μ to the first equation of (2) and integrate by part to have the following energy estimate:

$$\begin{aligned}\int_0^{T^*}\left((1-c_2\varepsilon U)\int_\Omega |\nabla\mu|^2 d\mathbf{x} + \alpha\int_{\partial\Omega} |\varepsilon\partial_{\mathbf{n}}\phi + \ell'(\phi)\cos(\theta_Y(x))|^2 ds\right) dt \\ \le \varepsilon E(\phi_0) + \varepsilon c_1 U T^* \le \varepsilon(E(\phi_0) + c_1 c_0),\end{aligned} \tag{8}$$

with $E(\phi) = \int_\Omega(\varepsilon|\nabla\phi|^2 + \frac{F(\phi)}{\varepsilon})\mathrm{d}\mathbf{x} + \int_{\partial\Omega}\gamma(\phi)\mathrm{d}s$. When ε goes to zero, we have $\nabla\mu$ convergence to zero. This implies that μ approaches to a constant in the leading order. We have the following expansion for μ:

$$\mu(x,t) = \mu_0(t) + \varepsilon\mu_1(x,t) + \cdots.$$

Remark 1. The fact that the leading order of μ is a constant can also be derived formally from asymptotic analysis[5], without using the energy estimate (8).

Sharp interface limit. Next we study the sharp interface limit as $\varepsilon \to 0$ for the solution of equations (2) and (3). Consider the matched asymptotic expansion as in [10][9]:

The outer expansion. Let $\Gamma^\varepsilon = \{\mathbf{x}|\phi(\mathbf{x}) = 0\}$. Suppose that far from the interface, the phase field function has the expansion

$$\phi = \phi_0 + \varepsilon\phi_1 + \cdots.$$

Substitute into the equation (2), we have, in the leading order, $F'(\phi_0) = 0$ which leads to $\phi_0 = \pm 1$. We denote $\Omega^\pm = \{\mathbf{x}|\phi_0(\mathbf{x},t) = \pm 1\}$.

The inner expansion. Suppose $\Gamma^\varepsilon(t)$ approaches to an interface $\Gamma^0(t)$ when ε goes to zero. We can do expansion near $\Gamma^0(t)$. Let $d(\mathbf{x})$ be the signed distance function to Γ_0. The our normal $\mathbf{m}$ and the signed curvature κ of the interface is given by

$$\mathbf{m} = \nabla d, \qquad \kappa = \Delta d.$$

We introduce the stretched variable near the interface Γ_0,

$$\xi = d(\mathbf{x})/\varepsilon.$$

Assume that ϕ and μ can be written in variable $(\mathbf{x},\xi,t)$ with expansions:

$$\begin{aligned}\phi &= \tilde\phi_0(\mathbf{x},\xi,t) + \varepsilon\tilde\phi_1(\mathbf{x},\xi,t) + \cdots \\ \mu &= \mu_0(t) + \varepsilon\tilde\mu_1(\mathbf{x},\xi,t) + \cdots.\end{aligned}$$

Here we use the fact that μ is a constant in the leading order. Given $\phi(\mathbf{x},t) = \phi(\mathbf{x},\xi,t), \mu(\mathbf{x},t) = \mu(\mathbf{x},\xi,t)$, the derivatives appearing in (2) transform according

to

$$\nabla\phi = \nabla_{\mathbf{x}}\phi + \varepsilon^{-1}\mathbf{m}\partial_\xi\phi,$$
$$\Delta\phi = \varepsilon^{-2}\partial_{\xi\xi}\phi + \varepsilon^{-1}\kappa\partial_\xi\phi + \Delta_{\mathbf{x}}\phi.$$

Substitute the expansions into the equation (2). The leading order is then given by

$$\partial_{\xi\xi}\tilde{\phi}_0 + \tilde{\phi}_0(\tilde{\phi}_0^2 - 1) = 0.$$

By matching condition that $\lim_{\xi\to\pm\infty}\tilde{\phi}_0 = \pm 1$, we know that the solution of the above equation is unique and independent of x and t:

$$\tilde{\phi}_0(\mathbf{x}, \xi, t) = \tanh(\xi/\sqrt{2}) =: Q(\xi).$$

The next order expansion leads to

$$\partial_{\xi\xi}\tilde{\phi}_1 + \tilde{\phi}_1(\tilde{\phi}_0^2 - 1) = \mu_0 + \kappa\partial_\xi\tilde{\phi}_0.$$

The solvability condition leads to

$$\sigma\kappa + \mu_0 = 0,$$

with $\sigma = \int_{-\infty}^{\infty}(\partial_\xi Q)^2 \mathrm{d}\xi = \int_{-1}^{1}\sqrt{2F(s)}\mathrm{d}s = 2\sqrt{2}/3$. Since $\mu_0(t)$ is a constant for any given t, we know that the curvature of the interface Γ_0 is constant for any given t.

Interface and contact angle dynamics. We now consider the expansion near the contact point. Suppose the domain Ω is a channel as shown in Figure 2. From the analysis above, we can assume that the limiting interface Γ^0 be a circle centered at $(a(t), 0)$ with radius $R(t)$:

$$\Gamma_t^0 = \{(a(t), 0) + R(t)(\cos\vartheta, \sin\vartheta); |\vartheta| \le \beta(t)\}$$

Denote the zero level set Γ_t^ε of ϕ^ε as

$$\Gamma_t^\varepsilon = \{(a(t), 0) + R^\varepsilon(\vartheta, t)(\cos\vartheta, \sin\vartheta); |\vartheta| \le \beta^\varepsilon(t)\}$$

We can assume the expansion

$$R^\varepsilon(\vartheta, t) \sim R(t) + \varepsilon R_1(\vartheta, t) + \varepsilon^2 R_2(\vartheta, t) + ...$$

We use the the stretched variable $(x, y) \to (\eta, z)$ defined by

$$\eta = \frac{y+H}{\varepsilon}, \quad z = \frac{r - R^\varepsilon(\vartheta, t)}{\varepsilon} \quad \Big(r = \sqrt{(x-a(t))^2+y^2}, \quad \vartheta = \arctan\frac{y}{x-a(t)}\Big).$$

and seek the following expansions:

$$\phi = \Phi^0(z, \eta, t) + \varepsilon\Phi^1(z, \eta, t) + \cdots,$$
$$\mu = \mu_0(t) + \varepsilon\hat{\mu}_1(z, \eta, t) + \cdots,$$
$$\beta = \beta(t) + \varepsilon\beta^1(t) + \cdots$$

Notice also the expansion of the differential operators:

$$\partial_x = \varepsilon^{-1}\cos\vartheta\partial_z, \qquad \partial_y = \varepsilon^{-1}(\partial_\eta + \sin\vartheta\partial_z),$$
$$\partial_t = \varepsilon^{-1}(-a_t\cos\vartheta - R_t)\partial_z + \partial_t.$$

Substitute the expansions into the equation (2) and the boundary condition (3). The leading order expansion becomes

$$\begin{cases} \Phi^0_{zz} + 2\sin\beta\, \Phi^0_{\eta z} + \Phi^0_{\eta\eta} - F(\Phi^0) = 0 & \forall\, z \in \mathbb{R}, y > -H, \\ \Phi^0(z,\infty,t) = \tilde{\phi}_0(z), & \forall\, z \in \mathbb{R}, \\ (-a_t\cos\beta - R_t + \alpha\sin\beta)\Phi^0_z & \\ \quad = \alpha[\Phi^0_\eta - \cos(\theta_Y(x))\ell'(\Phi^0)] & \forall z \in \mathbb{R}, y = -H. \end{cases} \tag{9}$$

We can easily see that $\Phi_0(z,\eta,t) = Q(z)$ is an explicit solution and since

$$\ell'(Q) = \partial_z Q,$$

we have, from the last equation of (9)

$$-a_t\cos\beta - R_t = -\alpha(\sin\beta + \cos(\theta_Y(x))). \tag{10}$$

Suppose the height of the channel is $2H$ and the length is L, i.e. $\Omega = (0,L)\times(-H,H)$. We have the following geometric relation:

$$H = R\sin\beta, \tag{11}$$

$$R^2(\beta - \sin\beta\cos\beta) + 2H(a + R\cos\beta) = A, \tag{12}$$

where A is the volume of phase 1 (left of the interface) in the channel. From (7), it is easy to show that

$$\frac{dA}{dt} = 2HU. \tag{13}$$

We can then deduce from (10), (11) and (12) that

$$\begin{cases} \beta_t = \Big[-\alpha\frac{\sin\beta+\cos(\theta_Y(x))}{H\cos\beta} + \frac{U}{H}\Big] g(\beta), \\ \\ x_t = \alpha\frac{\sin\beta+\cos(\theta_Y(x))}{\cos\beta}. \end{cases} \tag{14}$$

where $g(\beta) = \frac{\sin^3(\beta)}{(\sin\beta - \beta\cos\beta)}$, $x(t) = a(t) + R(t)\cos\beta(t)$ is the position of the contact point.

It is more convenient to choose the contact angle θ as unknown instead of β. Notice that $\beta = \theta - \frac{\pi}{2}$ (see Figure 2). Also denote non-dimensionalized channel length $\hat{L} = \frac{L}{H}$ and use rescaled parameters $\hat{\alpha} = \frac{\alpha}{H}$, the rescaled the contact point position $\hat{x} = \frac{x}{H}$ and the rescaled velocity $v = U/H$, the equation (14) can be rewritten as

$$\begin{cases} \theta_t = \Big[\hat{\alpha}\frac{\cos\theta - \cos(\hat{\theta}_Y(\hat{x}))}{\sin\theta} + v\Big]\tilde{g}(\theta), \\ \\ \hat{x}_t = -\hat{\alpha}\frac{\cos\theta - \cos(\hat{\theta}_Y(\hat{x}))}{\sin\theta}. \end{cases} \tag{15}$$

Here $\tilde{g}(\theta) = \frac{\cos^3(\theta)}{\cos\theta + (\theta - \frac{\pi}{2})\sin\theta}$ and $\hat{\theta}_Y(\hat{x}) = \theta_Y(H\hat{x})$.

3. **Contact angle hysteresis.**

In this section, we will study the behavior of the solution to equation (15) and show that, for the chemically patterned surface, the equation can describe the stick-slip behavior and contact angle hysteresis. For

simplicity, we use α, x and θ_Y instead of $\hat{\alpha}$, $\hat{x}$ and $\hat{\theta}_Y$. The equation (15) is rewritten as

$$\begin{cases} \theta_t = \Big[\alpha \frac{\cos\theta - \cos(\theta_Y(x))}{\sin\theta} + v\Big]\tilde{g}(\theta), \\ x_t = -\alpha \frac{\cos\theta - \cos(\theta_Y(x))}{\sin\theta}, \end{cases} \tag{16}$$

where $\tilde{g}(\theta) = \frac{\cos^3(\theta)}{\cos\theta + (\theta - \frac{\pi}{2})\sin\theta}$. When $v > 0$, we have an advancing interface and when $v < 0$, we have a receding interface.

We consider only the partial wetting situation, which means that the contact angle of the two-phase flow system is in the interval $\theta \in (0, \pi)$. It is easy to see $\tilde{g}(\theta)$ is monotone increasing in $(0, \pi/2]$ and monotone decreasing in $[\pi/2, \pi)$, satisfying $1 \le \tilde{g}(\theta) \le 3$.

We first look at the case when the solid surface is homogeneous. We have the following Theorem.

Theorem 3.1. *Suppose the solid surface is homogeneous, i.e. $\theta_Y(x) = \theta_Y$ is a constant. The solution of (16), $(\theta(t), x(t))$ has the following property:*

(1). If $v = 0$, we have

$$\theta(t) \to \theta_Y \text{ and } x(t) \to x_0 \text{ exponentially, as } t \to \infty,$$

i.e. the interface approaches to an equilibrium with contact angle θ_Y and contact point x_0.

(2). If $v \neq 0$ and $|v|$ is small, the contact angle $\theta(t)$ will converge to an equilibrium value $\theta^*(v, \theta_Y)$, which is speed v dependent. Furthermore, the contact point velocity approaches a constant, i.e. $\lim_{t\to\infty} x_t(t) = v$.

Proof. By (15), if $v = 0$, we easily have

$$\frac{d}{dt}(\cos\theta - \cos\theta_Y) = -\alpha(\cos\theta - \cos\theta_Y)\tilde{g}(\theta).$$

Since $1 \le \tilde{g} \le 3$, we have that

$$|\cos\theta(t) - \cos\theta_Y| \le |\cos\theta(0) - \cos\theta_Y| e^{-\alpha t} \to 0$$

By the second equation of (16), $x_t \to 0$ exponentially when $\theta \to \theta_Y$. Therefore the contact position x approaches to a stationary position x_0. This proves (1).

If $v \neq 0$, denote

$$F_1(\theta) = \Big[\alpha \frac{\cos\theta - \cos(\theta_Y)}{\sin\theta} + v\Big]\tilde{g}(\theta),$$
$$F_2(\theta) = -\alpha \frac{\cos\theta - \cos(\theta_Y)}{\sin\theta}.$$

Let $\theta^*(v, \theta_Y)$ be the root of $F_1(\theta) = 0$ (which is unique in $(0, \pi)$). From Taylor expansion of F_1 near θ_Y, we have

$$F_1 = \Big[-\alpha(\theta - \theta_Y) + v + o(\theta - \theta_Y) + ...\Big]\tilde{g}(\theta).$$

When $\frac{|v|}{\alpha}$ is small enough, the equation $F_1 = 0$ has a solution

$$\theta^* \approx \theta_Y + \frac{v}{\alpha}.$$

Furthermore, θ^* is a monotone increasing function of θ_Y and v.

Notice that when $\theta = \theta^*$, we have $F_2 = v$, or $x_t = v$, in other words, the contact point x will move with a constant velocity v. □

Since the ODE system (16) is autonomous, we can also study the behavior of the solution by phase-plane analysis. For the homogeneous surface, we plot the phase planes of the system (16) in Figure 3, in which the θ nullcline (the curve along which $\theta_t = 0$) and the x nullcline (the curve along which $x_t = 0$) are also shown. The θ nullcline is given by $\theta = \theta^*$ and the x nullcline is given by $\theta = \theta_Y$. The Figure 3 (a) is for $v > 0$ where $\theta^* > \theta_Y$, and the Figure 3 (b) is for $v < 0$ where $\theta^* < \theta_Y$. It is easy to see from the behavior of the vector field that $\theta = \theta^*$ is an attractor of all trajectories (blue curves). That is, the contact angle θ approaches to θ^* as $t \to \infty$. This verifies our analysis in Proposition 2.

In fact, more information can be extracted from the phase-plane analysis. Take the case $v > 0$ for example (see Figure 3(a)), the θ-nullcline is given by $\theta = \theta^*$. The x-nullcline is give by $\theta = \theta_Y$. Notice that

$$\frac{\mathrm{d}\theta}{\mathrm{d}x} = \frac{F_1}{F_2} = (-1 - \frac{v \sin\theta}{\alpha(\cos\theta - \cos\theta_Y)})\tilde{g}(\theta) = G(\theta), \tag{17}$$

is independent of x. Therefore, all uniclines, i.e. the curves along which the trajectories have the same slope $G(\theta)$, are parallel to x axis. Furthermore, when v is small, we can also see that $G(\theta)$ is a monotone decreasing function of θ. If $\theta > \theta^*$, we have $0 > G(\theta) > -3$ (recall that $3 > \tilde{g}(\theta) > 1$)). If $\theta < \theta_Y$, $G(\theta)$ goes from -3 to $-\infty$. If $\theta_Y < \theta < \theta^*$, $G(\theta)$ goes from $+\infty$ to 0. The region bounded by θ-nullcline and the x-nullcline is an attracting region, i.e. all trajectories will be attracted to the region and approach to $\theta = \theta^*$.

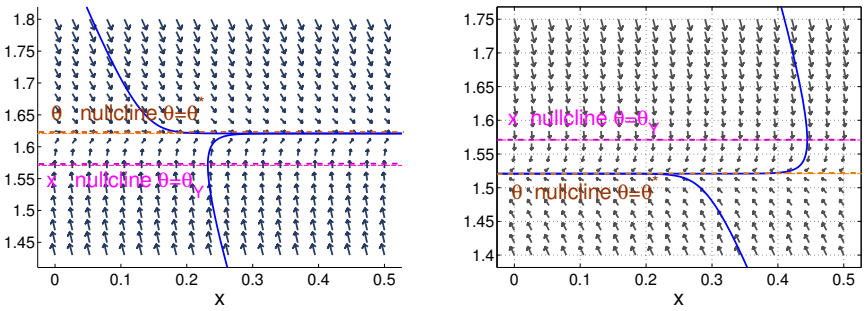

(a) $v > 0$ (b) $v < 0$

FIGURE 3. The phase plane for the homogeneous boundary

To study contact angle hysteresis, we consider a periodically patterned surface (Fig.2) specified by a piecewise constant periodic function $\bar{\theta}_Y(x)$ with period 1,

$$\bar{\theta}_Y(x) = \begin{cases} \theta_{Y1} & 0 < x \le \frac{1}{2}; \\ \theta_{Y2} & \frac{1}{2} < x \le 1; \end{cases} \tag{18}$$

where $\theta_{Y1} < \theta_{Y2}$. We then smooth out the discontinuity using linear interpolation within a thin region of size $2\delta(\delta << 1)$ around the discontinuity and define a continuous periodic function

$$\tilde{\theta}_Y(x) = \begin{cases} \theta_{Y1} & \delta \le x < \frac{1}{2} - \delta; \\ \theta_{Y1} + (x - \frac{1}{2} + \delta)(\theta_{Y2} - \theta_{Y1})/2\delta & \frac{1}{2} - \delta \le x \le \frac{1}{2} + \delta \\ \theta_{Y2} & \frac{1}{2} + \delta < x \le 1 - \delta; \\ \theta_{Y2} - (x - 1 + \delta)(\theta_{Y2} - \theta_{Y1})/2\delta & 1 - \delta \le x \le 1 + \delta \end{cases} \tag{19}$$

We now introduce a periodically patterned surface with $\theta_Y(x) = \tilde{\theta}_Y(\frac{x}{T})$ in system (16) with the period of the pattern T.

With the periodic pattern defined by the piecewise constant function $\bar{\theta}_Y(x)$ in (18), the coresponding phase plane can be obtained by piecing together periodically the phase plane in Fig. 3 where θ nullcline and x nullcline are pirecewise constants. With the smoothed $\tilde{\theta}_Y(x)$ in (19), the corresponding phase plane is given in Fig. 4 where the θ nullcline and x nullcline are smoothly connected as shown in Fig.4 (b). We denote $\theta_1^* = \theta_1^*(v, \theta_{Y1})$, $\theta_2^* = \theta_2^*(v, \theta_{Y2})$ the dynamic contact angles (defined in Theorem 3.1) on surface with Young's angle θ_{Y1}, θ_{Y2} respectively. We also have $\theta_1^* < \theta_2^*$ for $|v|$ small.

The following theorem gives the behavior of the contact angle $\theta(t)$ and contact point $x(t)$ on the patterned surface and their dependence on speed v.

Theorem 3.2. *For the chemically patterned surface with $\theta_Y(x) = \tilde{\theta}_Y(\frac{x}{T})$ given above and assuming interface speed v small, the solution $(\theta(t), x(t))$ of system (16) satisfies the following properties which display the stick-slip behaviour and contact angle hysteresis.*

(a). For period T large enough, $\theta(t)$ is a periodic function with $\theta_1^* \le \theta(t) \le \theta_2^*$ after an initial transient time, as the contact point $x(t)$ moves forward ($v > 0$) or backward ($v < 0$).

(b). For T small and $v > 0$, there exists a $\hat{\theta}_1(T)$ such that $\hat{\theta}_1(T) \le \theta(t) \le \theta_2^*$ after an initial transient time, and $\hat{\theta}_1(T) \to \theta_2^*$ as $T \to 0$.

(c). For T small and $v < 0$, there exists a $\hat{\theta}_2(T)$ such that $\theta_1^* \le \theta(t) \le \hat{\theta}_2(T)$ after an initial transient time, and $\hat{\theta}_2(T) \to \theta_1^*$ as $T \to 0$.

Proof. We will prove only the statement for $v > 0$. The case $v < 0$ can be proved in a similar way. The proof is based on a phase-plane analysis for $x - \theta$ plane in Figure 4(a).

We define two curves C_1 and C_2 which are the θ-nullcline and x-nullcline respectively (see Figure 4(b)):

$$C_1 := \{(x, \theta) | F_1(x, \theta) = 0, T\delta < x < T(1 + \delta)\},$$
$$C_2 := \{(x, \theta) | F_2(x, \theta) = 0, T\delta < x < T(1 + \delta)\}.$$

It is easy to show from phase plane analysis that the region I:

$$I = \{(x, \theta) \mid \text{bounded by } C_1, C_2 \text{ and } x = T\delta, x = T(1 - \delta), \}$$

is an attracting region. Any trajectory starting from a point (x, θ) within the boxed region (Fig. 4 (a)) will be attracted to region I and can only escape at the right end of the region at $x = T(1 - \delta)$. We denote the very thin layer (recall that $\delta << T$) around the point $x = T/2$ as

$$S = \{(x, \theta) \in I |\ T(\frac{1}{2} - \delta) < x < T(\frac{1}{2} + \delta)\ \}$$

which is a 'stick region' in which θ changes quickly from near θ_1^* to near θ_2^* as x moves slowly across (or pinned at) the point $x = T/2$ (Figure 4(b)).

Suppose a trajectory leaves the stability region between C_1 and C_2 at, without loss of generality, the end point $(T(1-\delta), \theta_2^*)$, and arrives quickly at $(T(1+\delta), \theta_2^*)$. Then there will be two possibilities depending on the size of T (the period of the pattern). Denote

$$\rho := G_1(\theta_2^*) = (-1 - \frac{v \sin \theta_2^*}{\alpha(\cos \theta_2^* - \cos \theta_{Y1})})\tilde{g}(\theta_2^*)$$

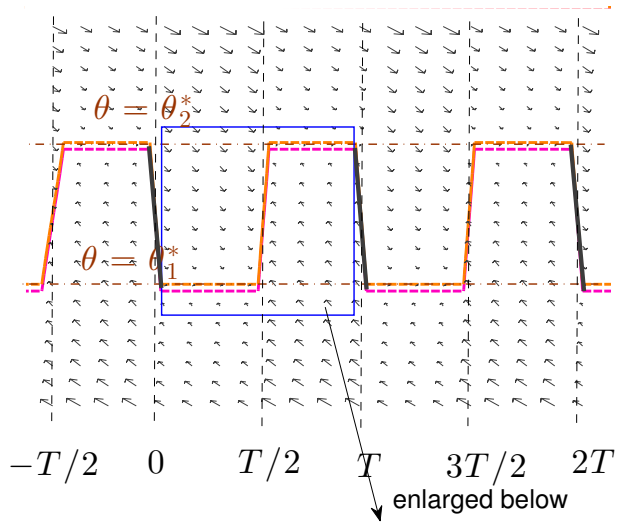

(a) the phase plane

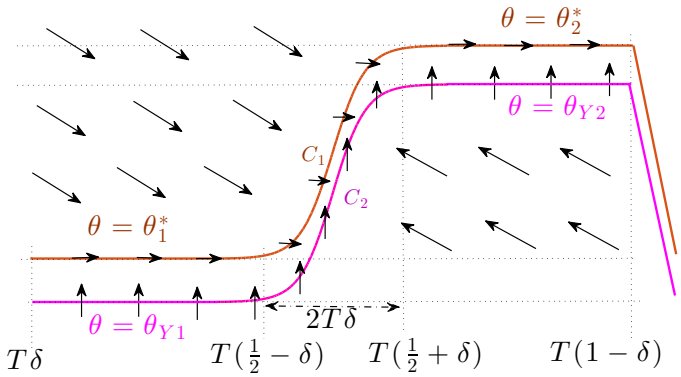

(b) the attracting region.

FIGURE 4. The phase plane and the attracting region bounded by the nullclines.

the slope of a trajectory on unicline $\theta = \theta_2^*$ in material 1(see Equation (17)). Then we have that $-3 < \rho < 0$ and is independent of T. We can draw a straight line at the point $(T(1+\delta), \theta_2^*)$ with the slope equal to ρ (the blue lines in Figure 5).

Case 1: When $T > \frac{2(\theta_2^* - \theta_1^*)}{(-\rho)}$ and large enough, the trajectory will reach $\theta = \theta_1^*$(Figure 5(a)). In this case, the contact angle completely switches from θ_2^* to θ_1^*. The trajectory 'slips' until it hits the 'stick region' S in the next period and climbs from θ_1^* to θ_2^*.

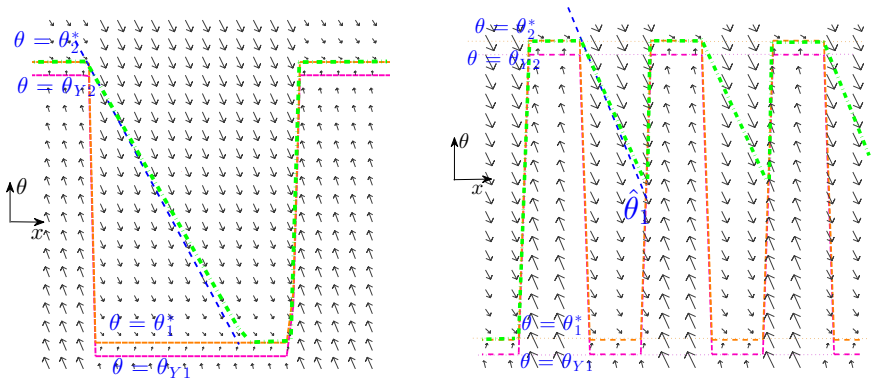

(a) T large (b) T small

FIGURE 5. The advancing contact angle trajectory for large (left) and small (right) pattern period T.

Case 2: When $T < \frac{2(\theta_2^* - \theta_1^*)}{(-\rho)}$, the trajectory will hit the next 'stick region' S at some $\theta > \hat{\theta}_1(T) := \theta_2^* + \frac{\rho T}{2}$ (Figure 5(b)). Therefore, a complete switch will not happen. It is easy to see that as T becomes small, $\hat{\theta}_1(T)$ approaches to θ_2^*

In either case, the process then repeats periodically and we have $\max(\theta_1^*, \hat{\theta}_1) < \theta < \theta_2^*$. When T is small enough, only Case 2 happens and as $T \to 0$, we have $\lim_{T \searrow 0} \hat{\theta}_1 \nearrow \theta_2^*$. □

From the above phase analysis, we have the following conclusions. For periodic chemically patterned boundary, the interface will move with a stick-slip behaver (after an initial transient period). When the period T of the pattern is small, we have contact angle hysteresis, i.e., for $v > 0$, the advancing angle is approaching to $\theta_2^*(v)$, which is lager than θ_{Y2} and for $v < 0$, the receding angle is approaching to $\theta_1^*(v)$, which is smaller than θ_{Y1}. In addition, when v goes to zero, the $\theta_1^*(v)$ increases to θ_{Y1} and $\theta_2^*(v)$ decreases to θ_{Y2}.

4. **Numerical Examples.** In this section, we will verify the above theory with some numerical examples. The first example is for a channel with periodically patterned boundary with two materials of contact angle $\theta_{Y1} = \pi/3 \approx 1.05$ and $\theta_{Y2} = 2\pi/3 \approx 2.09$ respectively. We set $\alpha = 10$ and $v = \pm 0.5$ and solve the ODE (16) numerically. The numerical results are shown in Figure 6. In the left subfigure, we show the advancing and receding trajectories (θ, x) for the pattern period $T = 2\pi/5$; and in the right one we show that for $T = 2\pi/40$. We can see that both trajectories have periodic oscillating behavior. When T is small, we observe obvious contact angle hysteresis. Due to the velocity $v \neq 0$, the advancing angle θ_2^* is slightly larger than θ_{Y2} and the receding angle θ_1^* is slightly smaller than θ_{Y1}. We also plot the contact point velocity x_t for the advancing trajectory in Fig. 7 which shows the stick-slip behaviour of the contact point. The contact

point sticks (with a velocity close to zero) as it reaches the intersection point A from the hydrophilic part, while the contact point slips (with a large slip velocity) as it passes the intersection point B from hydrophobic side. The stick-slip behaviour is more evident in the log scale plot of the contact point velocity x_t in Fig. 7.

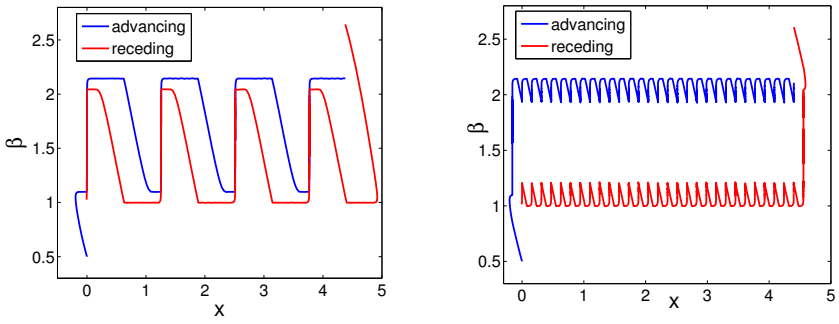

(a) $T = 2\pi/5$. (b) $T = 2\pi/40$

FIGURE 6. Advancing and receding contact angles for large ($T = 2\pi/5$) and small ($T = 2\pi/40$) pattern period. For large T, we observe stick-slip of the contact point (see Fig. 7). For small T, we observe contact angle hysteresis.

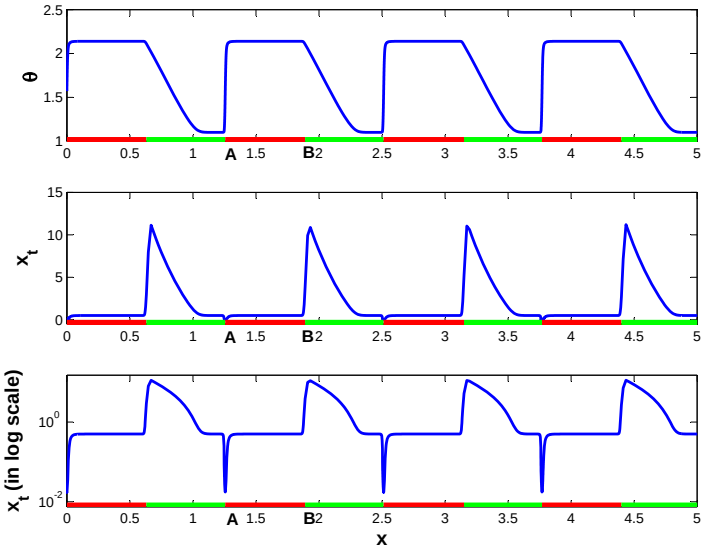

FIGURE 7. The contact point stick-slip behaviour for pattern surface with period $T = 2\pi/5$. Top: advancing trajectory of contact angle θ. Middle: contact point velocity x_t. Below: x_t in log scale

In the second example, we consider a channel with inhomogeneous boundaries, where $\theta_Y(x)$ is smooth function, instead of a piecewise constant function in the first

example. We set

$$\theta_Y(x) = \frac{\pi}{2} + \frac{\pi}{6}\sin(kx),$$

and again with $\alpha = 10$ and $v = \pm 0.5$. The numerical results are shown in Figure 8. The left subfigure shows the trajectories for $k = 5$ (i.e. the period $T = 2\pi/5$), and the right one shows those for $k = 40$ (i.e. $T = 2\pi/40$). Again, when T is small, we observe contact angle hysteresis. The advancing angle and receding angle are the same as in last example.

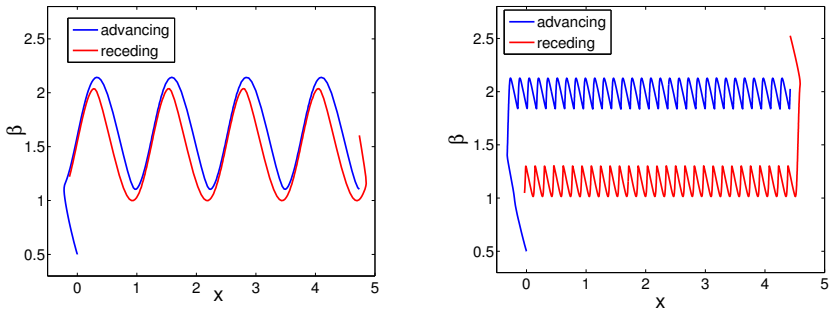

(a) $T = 2\pi/5$. (b) $T = 2\pi/40$

FIGURE 8. Advancing and receding contact angles for inhomogeneous surfaces with smooth θ_Y with large and small patterned period.

REFERENCES

[1] P.G. de Gennes. Wetting: Statics and dynamics. *Rev. Mod. Phys.*, 57:827–863, 1985.
[2] T. Young. An essay on the cohesion of fluids. *Philos. Trans. R. Soc. London*, 95:65–87, 1805.
[3] Antonio DeSimone, Natalie Gruenewald, and Felix Otto. A new model for contact angle hysteresis. *Networks and heterogeneous media*, 2:211–225, 2007.
[4] Alessandro Turco, Franois Alouges, and Antonio DeSimone. Wetting on rough surfaces and contact angle hysteresis: numerical experiments based on a phase field model. *ESAIM: Mathematical Modelling and Numerical Analysis*, 43:1027–1044, 11 2009.
[5] X. Xu and X. P. Wang. Analysis of wetting and contact angle hysteresis on chemically patterned surfaces. *SIAM J. Appl. Math.*, 71:1753–1779, 2011.
[6] T. Qian, X.P. Wang, and P. Sheng. Molecular scale contact line hydrodynamics of immiscible flows. *Phys. Rev. E*, 68:016306, 2003.
[7] T. Qian, X.P. Wang, and P. Sheng. Power-law slip profile of the moving contact line in two-phase immiscible flows. *Phys. Rev. Lett.*, 93:094501, 2004.
[8] X.P. Wang, T. Qian, and P. Sheng. Moving contact line on chemically patterned surfaces. *Journal of Fluid Mechanics*, 605:59–78, 2008.
[9] X. Chen, X.-P. Wang, and X. Xu. Analysis of the cahnhilliard equation with a relaxation boundary condition modeling the contact angle dynamics. *Arch. Rational Mech. Anal.*, 213:1–24, 2014.
[10] R. Pego. Front migration in the nonlinear cahn-hilliard equation. *Proc. R. Soc. Lond., A*, 422:261–278, 1989.

Received xxxx 20xx; revised xxxx 20xx.

E-mail address: mawang@ust.hk
E-mail address: xmxu@lsec.cc.ac.cn